# Polymer Electrolytes for Potassium-based Batteries: Incorporating Ionic Liquids to Enhance the Room Temperature Ionic Conductivity

Jinyu Chen[a,b], Sohelia Ebrahimi[c], Boyan Iliev[d], Yuval Steinberg[e], Michal Leskes[e], Thomas J. S. Schubert[d], Elizabeth Castillo-Martínez[c], Dominic Bresser[a,b], Maider Zarrabeitia*[a,b]

[a] Helmholtz Institute Ulm (HIU), Helmholtzstasse 11, 89081 Ulm, Germany
[b] Karlsruhe Institute of Technology (KIT), P.O.Box 3640, 76021 Karlsruhe, Germany
[c] Department of Inorganic Chemistry, Universidad Complutense de Madrid, 28040, Madrid, Spain
[d] Iolitec Ionic Liquids Technologies GmbH, Im Zukunftspark 9, 74076 Heilbronn, Germany
[e] Department of Molecular Chemistry and Materials Science, Weizmann Institute of Science, Rehovot 761000, Israel

## EXPERIMENTAL DETAILS

### Structural characterisation

The structural properties of solvent-free SPEs were analysed by XRD using Bruker D8 Advance diffractometer in the 2θ range from 10° to 90° with a step size of 0.02°. PXRD of PW were collected with an Empirean Panalytical diffractometer in the 2θ range from 10° to 80° with a step size of 0.02°. PW was also investigated with FTIR, the FTIR spectra were collected by adding 4 scans in the 400-4000 $cm^{-1}$ wavenumber range with 4 $cm^{-1}$ resolution.

### Thermal characterisation

TGA (TG 209F1 Libra, Netzsch) and DSC (Discovery DSC, TA Instruments) were used to analyse the thermal stability and phase transition behaviour of solvent-free SPEs. All solvent-free SPE membranes were sealed in Al pans. TGA experiments were performed and underwent a 30 min isothermal step at 30 °C, followed by heating up to 600 °C at a rate of 5 K $min^{-1}$ under an inert $N_2$ atmosphere. In the case of DSC analysis, an isothermal equilibration step at 40 °C for 30 min was conducted, followed by one cooling and heating cycle between -100 °C and 100 °C. The cooling and heating rates were 5 K $min^{-1}$, and isothermal holds of 30 min were maintained at the turning points. All TGA and DSC measurements were performed in duplicate. The glass transition temperatures ($T_g$) were determined by the midpoint method, averaging the values obtained from all heating traces. By employing these experimental procedures, the thermal stability and phase transition behaviour of all solvent-free SPEs were effectively characterized, avoiding unnecessary repetition of steps.

### EIS for ionic conductivity calculation

Pouch-cell configuration was employed to construct symmetric Cu ‖ Cu blocking cells with a geometrical electrode area of 9 $cm^2$. The temperature-dependent conductivity of solvent-free SPEs was determined using EIS with a potentiostat-galvanostat (Solartron SI 1287, AMETEK) and a frequency response analyser (Solartron SI 1260, AMETEK), applying a 10 mV AC potential amplitude across a frequency range of 1 MHz to 1 Hz. For temperature control, the measurements were performed in a climatic chamber (Binder GmbH), and pouch cells were allowed to equilibrate for 3 h after a temperature change. A representative impedance spectrum and the equivalent circuit are used to fit the data.

### LSV for electrochemical stability window

The electrochemical stability of solvent-free SPEs was evaluated in two-electrode cells assembled in CR2032 coin-cell type utilising Al as a working electrode and K as a counter and reference electrode. LSV was performed to a lower limit of −2 V and an upper limit of 7 V vs $K^+/K$ at a scan rate of 0.1 mV $s^{-1}$ with a multi-channel potentiostat-galvanostat (VMP, Biologic Science Instruments).

**Stripping/plating for K compatibility (K ‖ QSPE ‖ K)**

To investigate the compatibility and stability of the interface between K and solvent-free SPEs, a stripping/plating test was conducted on symmetric K ‖ solvent-free SPE ‖ K cells. These cells were assembled in CR2032 coin-cell configuration and rested at open circuit voltage (OCV) for 6 h. The stripping/plating test was performed (1 h for each process) using a multi-channel potentiostat-galvanostat (VMP, Biologic Science Instruments) at 0.1 mA $cm^{-2}$ current density.

**EIS for K and PW compatibility (K ‖ solvent-free SPE ‖ K and K ‖ solvent-free SPE ‖ PW, respectively)**

EIS carried out the K and PW interface compatibility and stability in three three-electrode cells (El-Cell GmbH) with an AC potential amplitude of 10 mV and a frequency range of 1 MHz to 0.1 Hz.

The K ‖ solvent-free SPE interface was evaluated utilising K metal as the working, counter, and reference electrode. Step1: EIS tests initial interface impedance; step 2: resting at OCV for 6 h; step 3: EIS was conducted to measure the interfacial impedance of the contacted surfaces; step 4: the interfacial impedance was tested by EIS after 1 h stripping and 1 h plating at 100 μA $cm^{-2}$; step 5: the interfacial impedance was measured again by EIS; and step 6: repeat step 4- 5 till getting 100 cycles of stripping/plating.

The PW ‖ solvent-free SPE interface was evaluated utilising PW as the working electrode, K metal as the counter, and reference electrode. The same testing procedure was followed, except that instead of stripping/plating, the process was modified to include charge-discharge cycles (from 4.4 - 2.7 V vs $K^+/K$, at 0.1C). This modification allowed for a more comprehensive assessment of the cyclic performance and stability of the system under investigation. All tests are employed VMP.

**Electrochemical properties**

K-metal cells (K ‖ solvent-free SPE ‖ PW) were assembled in CR2032 coin-cells comprising 12 mm diameter K metal anodes, 15 mm diameter SPEs, and 12 mm diameter PW cathodes. The K metal was cut, roll pressed, and made into 12 mm diameter discs, following the literature [1]. After 6 h rest, galvanostatic cycling of the cells within a voltage range of 4.4 – 2.7 V vs $K^+/K$ was performed by using a Maccor 4000 battery tester applying a constant current of 15.5 mA $g^{-1}$ (1C, PW nominal capacity is 155 mAh $g^{-1}$). The cells were run at C-rates ranging from 0.1C to 1C. All electrochemical measurements were performed in climatic chambers (Binder GmbH) at 20 °C ± 2 °C, if not stated otherwise. To ensure good contact between the solvent-free SPEs and electrodes, a drop (20 μL) of K salt:IL solution (molar ratio of 1:4) corresponding to the particular solvent-free SPEs was applied at the PW interface.

**Chemical composition of SEI**

The surface chemistry of the K metal immersed for 28 days in KFSI:$Pyr_{12O1}$FSI and KTFSI:$Pyr_{12O1}$TFSI in a 1:4 molar ratio was investigated by using XPS. The XPS analyses were performed on a SPECS – Phoibos 150 XPS spectrometer and Surface concept micro-channel plate and delay line detector, using Al Kα monochromatic X-ray (hv = 1486.7 eV). High-resolution F 1s, K 2p, C 1s, and S 2p photoelectron regions were collected at low energies of 200 W, with 30 eV pass energy and 0.1 eV energy step. The K metal samples were prepared inside the glovebox, cutting a piece of K metal after being immersed for 28 days in the solution and transferred using an air-tight vessel directly to the XPS chamber without any contact with the atmosphere. The depth profiling was done using a focused ion gun for 5 keV $Ar^+$ with an ion filter and sputtering rate of 0.8 nm $min^{-1}$.

Solid state NMR measurements were performed on a Bruker Avance NEO 9.4 T spectrometer ($^1H$ Larmor frequency 400 MHz). The FSI:FSI and TFSI:TFSI were packed into a 2.5 mm rotor in the glove box. They were then transferred into the 2.5 mm triple resonance MAS probe for NMR measurements performed at 20 kHz MAS. $^1H$ and $^{19}F$ spectra were collected using a rotor-synchronized Hahn echo sequence, and $^{13}C$ spectra were acquired with a single pulse excitation followed by $^1H$ decoupling.

**Table S1.** The water content of K salts and ILs.

| | KFSI | KTFSI | $Pyr_{12O1}FSI$ | $Pyr_{12O1}TFSI$ |
|---|---|---|---|---|
| Water content (ppm) | 17.2 | 6.4 | 16.9 | 8.5 |

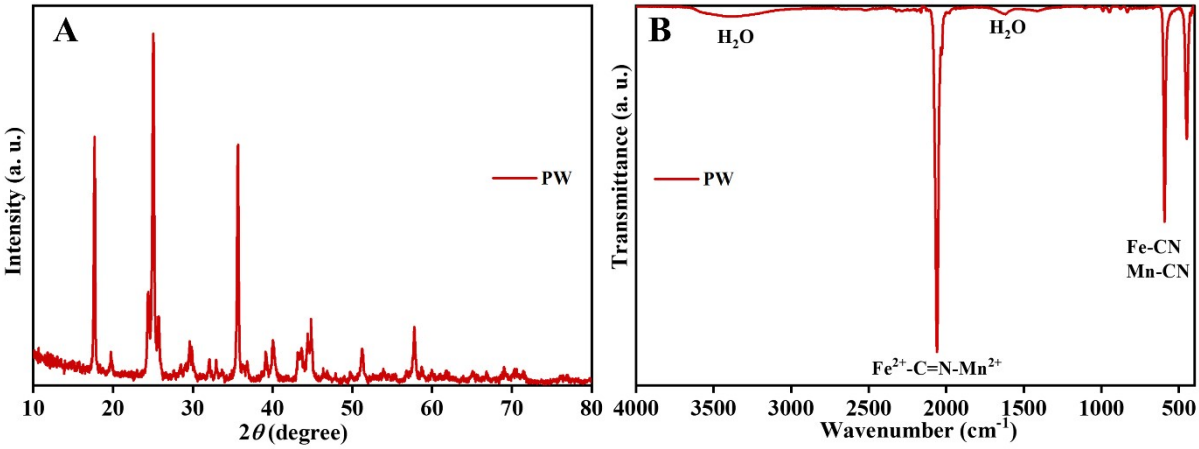


**Figure S1. A.** Powder XRD pattern and **B.** FTIR spectrum of PW.

The structural properties of PW are assessed using powder XRD, as shown in **Figure S1A**. The diffraction pattern reveals a sample where the most intense reflection of cubic PB around 25° 2 theta is split into three, indicating a monoclinic phase with $P2_1/n$ symmetry, consistent with findings from previous literature [2].

FTIR spectrum (**Figure S1B**) of the prepared PW displays distinct absorbance peaks at approximately 2060 and 592 $cm^{-1}$, corresponding to the stretching vibrations of C≡N and Fe–C≡N, respectively. These characteristic peaks confirm the formation of a Fe–C≡N–Mn octahedral structure. Additionally, the peak at 450 $cm^{-1}$ indicates the presence of the Mn–N bond within the PW structure [2].

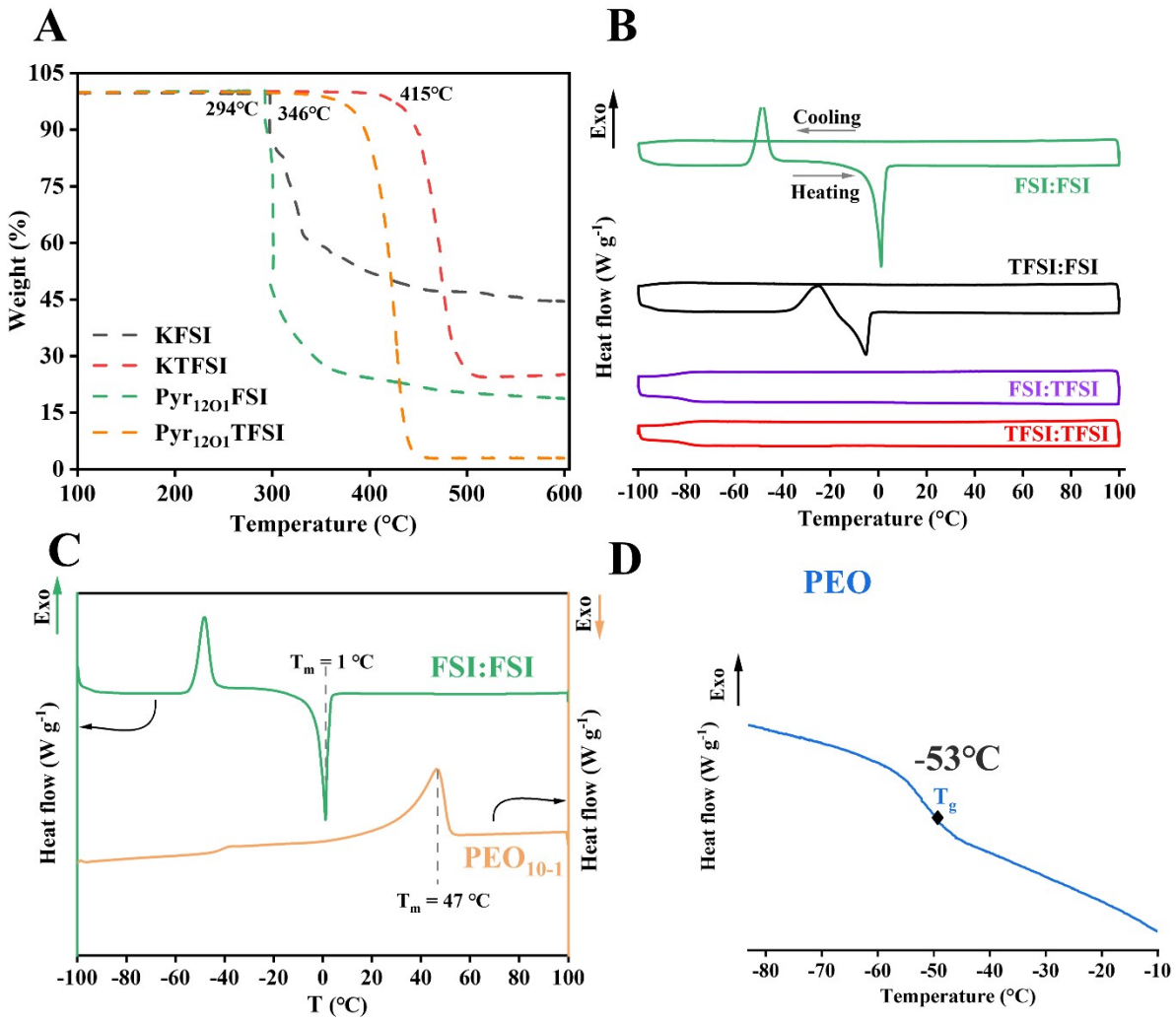


**Figure S2. A.** TGA curves of raw K salts and ILs, and **B.** DSC curves of all solvent-free SPEs, **C.** DSC curves of FSI:FSI and $PEO_{10-1}$ (cooling and heating cycles between -100 °C and 100 °C, cooling/heating rate of 5 K $min^{-1}$), and **D.** pure PEO.

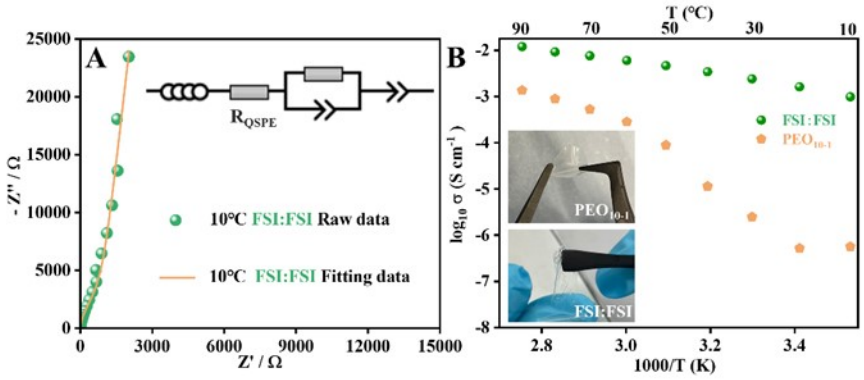


**Figure S3. A.** The Nyquist plot and the corresponding fitted curve of FSI:FSI at 10 °C. Inset: The used equivalent circuit model. B. Temperature-dependent ionic conductivity of FSI:FSI and PEO10-1, with illustrations of the two samples.

**Table S2.** Ionic conductivity comparison of different SPEs reported up to date.

| SPEs | Application topic | ILs added or not | $T_g$/°C | Ionic conductivity /mS $cm^{-1}$ | Ref. |
|---|---|---|---|---|---|
| **FSI: FSI** | KIBs | **YES** | **-94.0**<br>**-94.6** | **1.6 (20 °C)**<br>**6.0 (60 °C)** | **This work** |
| P(EO/MEEGE[a]/AGE[b])-KFSA | KIBs | NO | / | 0.02 (25 °C) | [1] |
| PEO + $KBrO_3$ (70:30) | KIBs | NO | / | $7.7 \times 10^{-5}$ (25 °C) | [5] |
| PEO + $KBPh_4$ (15:1) | KIBs | NO | ca. -25 | 0.11 (60 °C) | [6] |
| Polymer-gel electrolyte | KIBs | Contain organic-liquid electrolyte | / | 4.3 (RT[c]) | [7] |
| PPCB[d]-SPE + KFSI | KIBs | NO | / | 0.01 (20 °C) | [8] |
| BPE [e] $_{15}$-$NaTFSI_1$ | NIBs | NO | −45.4 | ca. 0.04 (25 °C) | [3] |
| FSI : FSI | NIBs | YES | −87 | 1.2 (20 °C) | (our previous work)[9] |
| PEO LiTFSI $Pyr_{14}FSI$ | LIBs | YES | −79.8 | ca. 0.3 (20°C) | [10] |
| PIL[f]- $Pyr_{14}$TFSI-LiTFSI | LIBs | YES | ca. -67 | 0.16 (20 °C)<br>0.48 (60 °C) | [11] |

[a] MEEG: 2-(2-methoxyethoxy)ethyl glycidyl ether;

[b] AGE: allyl glycidyl ether

[c] RT: room temperature

[d] PPCB: poly (propylene carbonate) (PPC)-KFSI with cellulose nonwoven backbone

[e] BPE: block copolymer-based electrolyte

[f] PIL: pyrrolidinium-based polymeric ionic liquid

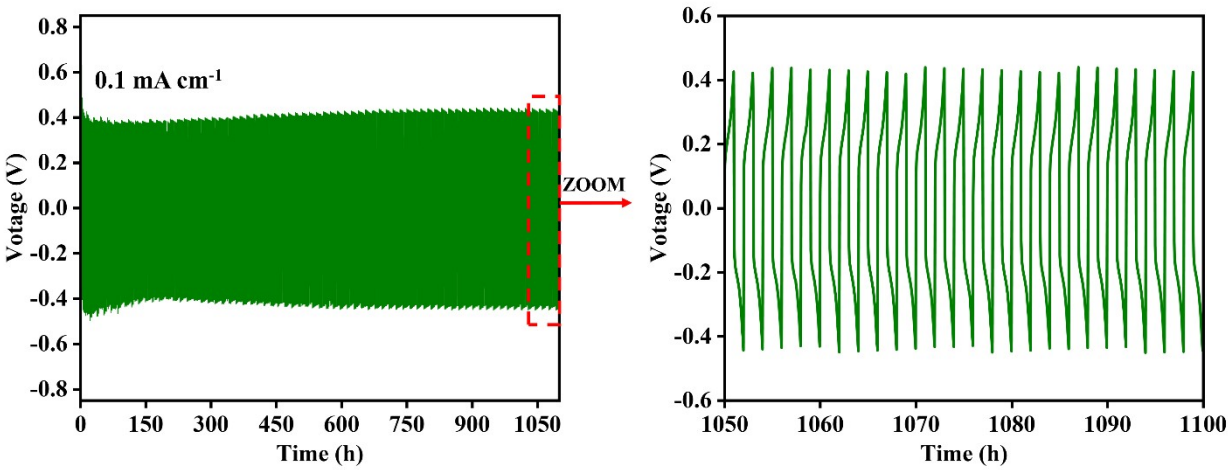


**Figure S4.** The stripping/plating cycles of K ‖ FSI:FSI ‖ K cell and the zooming curves of the last 20 cycles of the selected area (highlighted in red).

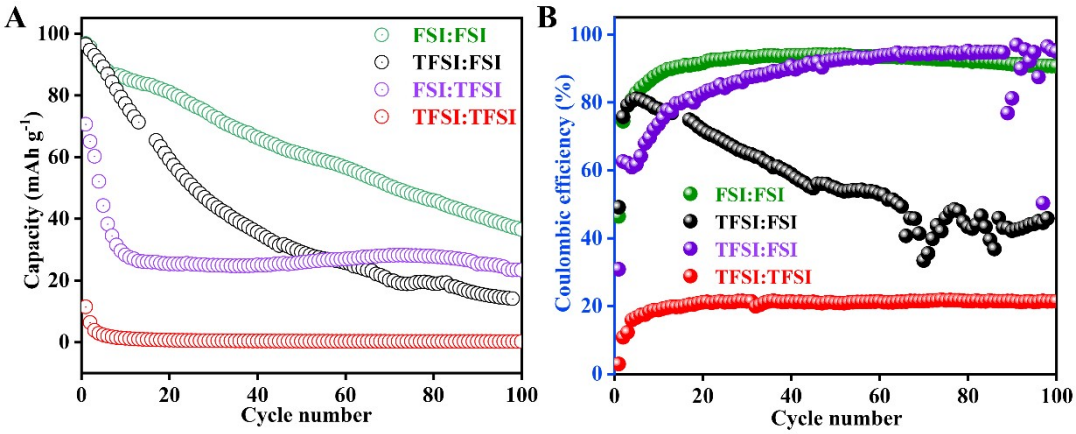


**Figure S5.** Capacity vs. cycle number of the K cell using PW as working and K as counter electrode between 4.4 - 2.7 V vs $K^+/K$ at 20 °C ± 2 °C). **A**. The discharge capacity of the K cells with solvent-free SPE at 0.1C and **B**. the corresponding CE.

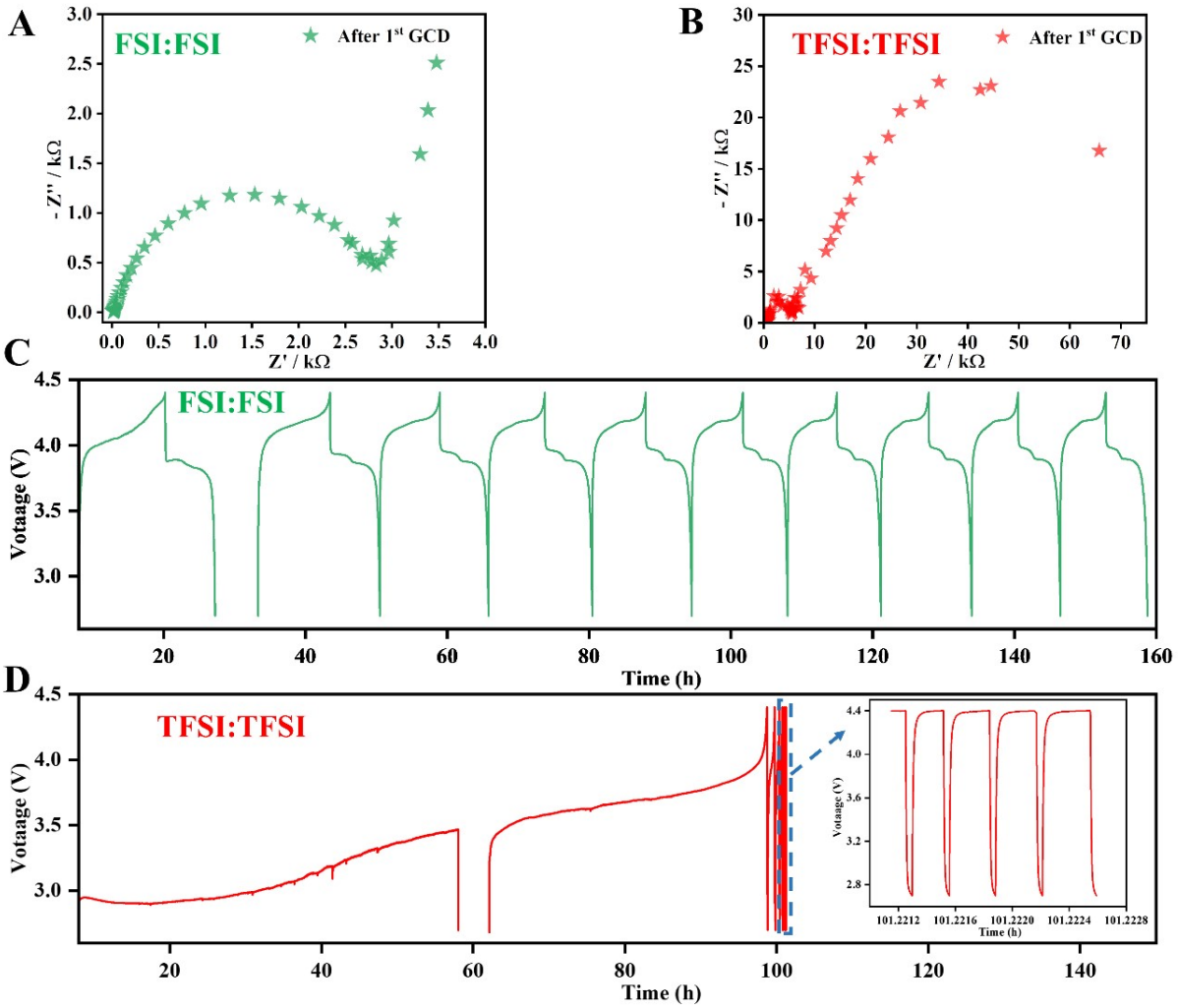


**Figure S6.** The Nyquist plots after the first GCD of **A.** FSI:FSI and **B.** TFSI:TFSI containing K cells. The galvanostatic 10 cycles of **C.** FSI:FSI, **D.** TFSI:TFSI-based cells. Inset: the last GCD of TFSI:TFSI. The charging and discharging steps were set to 50 h (even if the cell was run for more than 50 h, it did not achieve the upper cut-off voltage of 4.4V vs $K^+/K$).

**Reference**


1 M. Hamada, R. Tatara, K. Kubota, S. Kumakura and S. Komaba, *ACS Energy Lett.*, 2022, **7**, 2244–2246.

2 L. Deng, J. Qu, X. Niu, J. Liu, J. Zhang, Y. Hong, M. Feng, J. Wang, M. Hu, L. Zeng, Q. Zhang, L. Guo and Y. Zhu, *Nat. Commun.*, 2021, **12**, 1–9.

3 A. D. Khudyshkina, A. J. Butzelaar, Y. Guo, M. Hoffmann, T. Bergfeldt, M. Schaller, S. Indris, M. Wilhelm, P. Théato and F. Jeschull, *Electrochim. Acta*, 2023, **454**, 142421.

4 X. Dong, A. Mayer, Z. Chen, S. Passerini and D. Bresser, *ACS Energy Lett.*, 2024, 5279–5287.

5 T. Sreekanth, M. Jaipal Reddy and U. V. Subba Rao, *J. Power Sources*, 2001, **93**, 268–272.

6 M. Elmanzalawy, E. Sanchez-Ahijón, O. Kisacik, J. Carretero-González and E. Castillo-Martínez, *ACS Appl. Energy Mater.*, 2022, **5**, 9009–9019.

7 H. Gao, L. Xue, S. Xin and J. B. Goodenough, *Angew. Chemie Int. Ed.*, 2018, **57**, 5449–5453.

8 H. Fei, Y. Liu, Y. An, X. Xu, G. Zeng, Y. Tian, L. Ci, B. Xi, S. Xiong and J. Feng, *J. Power Sources*, 2018, **399**, 294–298.

9 D. Roscher, Y. Kim, D. Stepien, M. Zarrabeitia and S. Passerini, *Batter. Supercaps*, , DOI:10.1002/batt.202300092.

10 H. De Vries, S. Jeong and S. Passerini, *RSC Adv.*, 2015, **5**, 13598–13606.

11 G. B. Appetecchi, G. T. Kim, M. Montanino, M. Carewska, R. Marcilla, D. Mecerreyes and I. De Meatza, *J. Power Sources*, 2010, **195**, 3668–3675.